Chapter 3

INFLUENCE OF POLARISATION ON OCULAR ABERRATIONS

This chapter is based on the article by Marcos, S. et al.," Ocular aberrations with ray tracing and Shack–Hartmann wave-front sensors: Does polarisation play a role?", Journal of the Optical Society of America 19, 1063-1072 (2002b). The coauthors of the study are: Luis Diaz-Santana, Lourdes Llorente and Chris Dainty. The contribution of the author of this thesis to the study was the participation in the data collection and processing at Instituto de Óptica (LRT), as well as data and statistical analysis (HS and LRT).

3.1.- ABSTRACT

PURPOSE: To investigate whether polarisation may have an effect on reflectometric measurements of wave aberrations.

METHODS: Ocular aberrations were measured in 71 eyes by using two reflectometric aberrometers: LRT (60 eyes) and HS (11 eyes). The effect of different polarisation configurations in the aberration measurements, including linearly polarised light and circularly polarised light in the illuminating channel and sampling light in the crossed or

parallel orientations was studied. In addition, completely depolarised light in the imaging channel from retinal lipofuscin autofluorescence was studied for the HS measurements.

RESULTS: The intensity distribution of the retinal spots as a function of entry (for LRT) or exit pupil (for HS) depends on the polarisation configuration. These intensity patterns show bright corners and a dark area at the pupil centre for crossed polarisation, an approximately Gaussian distribution for parallel polarisation and a homogeneous distribution for the autofluorescence case. However, the measured aberrations are independent of the polarisation states.

CONCLUSIONS: These results indicate that the differences in retardation across the pupil imposed by corneal birefringence do not produce significant phase delays compared with those produced by aberrations, at least within the accuracy of these techniques. In addition, differences in the recorded aerial images due to changes in polarisation do not affect the aberration measurements in these reflectometric aberrometers.

3.2.- INTRODUCTION

Since polarised light interacts with the ocular optical components and the retina, the polarisation of the incident (and returning light in the imaging systems) might affect aberration measurements. Birefringence of the optical components of the eye, cornea (Van Blokland and Verhelst, 1987) and crystalline lens (Bueno and Campbell, 2001), produce a retardation of linearly polarised light (Van Blokland, 1986) (see Chapter 1, section 1.2.5.1). However, a published study (Prieto et al., 2001) using a psychophysical technique (SRR) showed no difference in the wave aberration measured with different states of polarisation of the illuminating channel suggesting that this retardation was negligible in terms of wavefront error. On the other hand, the use of polarisers in the

illumination and detection channels affects the intensity of the raw data (aerial retinal images captured on a CCD camera). Bueno and Artal (Bueno and Artal, 1999) used an ellipsometry approach to study the influence of polarization in double-pass estimates of the image quality of the eye. They found that the double-pass aerial image, autocorrelation of the ocular PSF (Artal et al., 1995), was influenced by the relative orientation of the polarizer and the analyzer (placed in the illumination channel and the imaging channel, respectively). These differences caused significant variations in the resulting modulation transfer function and therefore in the estimated image quality. Relative differences in intensity in the core and tails of the retinal image, or differences in shape could result in changes in the estimation of the centroid and have an impact on the wave aberration estimate.

In the work reported in this chapter the effect of polarisation on the intensity of the aerial images and on the wave aberration estimated from reflectometric measurements was studied. Data from a HS system (Chapter 1, section 1.2.3) implemented at the Imperial College, London, UK were analysed in combination to data obtained from the LRT described in the methods section (Chapter 2, section 2.1). The aim of this work was not to fully characterise the wave aberration with respect to state of polarisation, but rather to test whether some typical combinations of polarisation in the incident and detection channels may influence wave aberration measurements. These different combinations together with retardation across the pupil produce differences in the relative intensity of the aerial images captured. Additionally, a non-polarised condition was studied with the HS wavefront sensor. Our experiments show that these polarisation states do not influence reflectometric aberration measurements in the eye, at least within the error of the measurements.

3.3.- METHODS

3.3.1.- LASER RAY TRACING

3.3.1.1.- Setup and procedures

The device used in this study was LRT1 (see Chapter 2, section 2.2). A schematic diagram of the configuration of the device used in this work is shown in Figure 3.1. In order to induce the different polarisation conditions to study, a linear polarizer (LP) and a polarising cubic beam splitter (PCBS) were introduced in the setup, as well as a quarter wave plate (QWP) when required (see section 1.3.1.2).

3.3.1.2.- Experiments

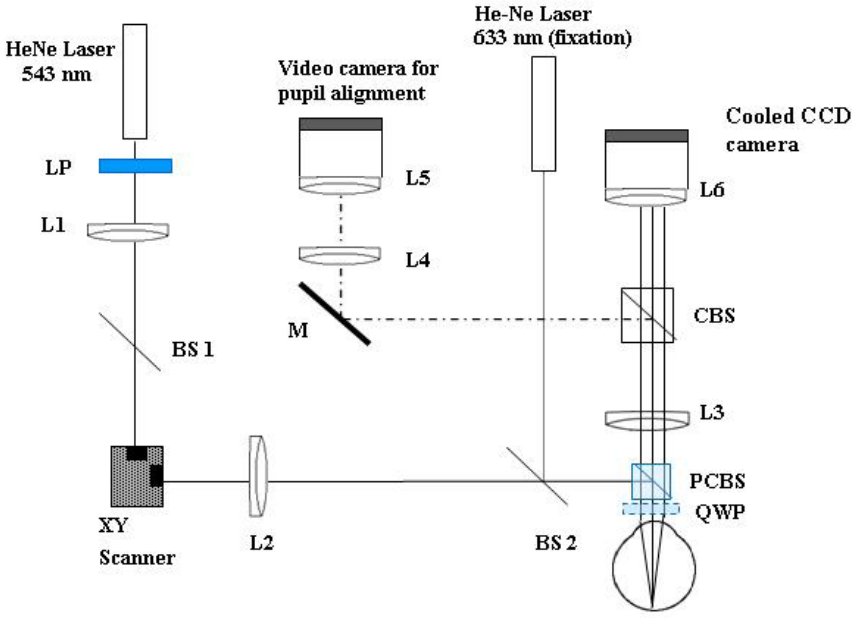

Figure 3.1. Schematic diagram of the configuration of LRT1 used in this study: LP is a linear polariser; L indicates lens; BS1 and BS2 are pellicle beam splitters; CBS is a cube beam splitter and M is a mirror. The polarising beam splitter (PCBS) and the quarter wave plate (QWP) contribute to obtain the different polarisation conditions.

Two different experiments were performed: 1) In the first one, the eye was illuminated with linearly polarised light and light was collected linearly polarised in the crossed direction. This was achieved by using a polarising beam splitter, which reflects linearly polarised light, and transmits linearly polarised light rotated 90º (see Figure 3.2 A). 2) In the second one, a quarter-wave plate was introduced between the polarising beam splitter and the eye. Light in the illumination channel was then circularly polarised, and light with the same state of polarisation was fully transmitted into the imaging channel (see Figure 3.2 B).

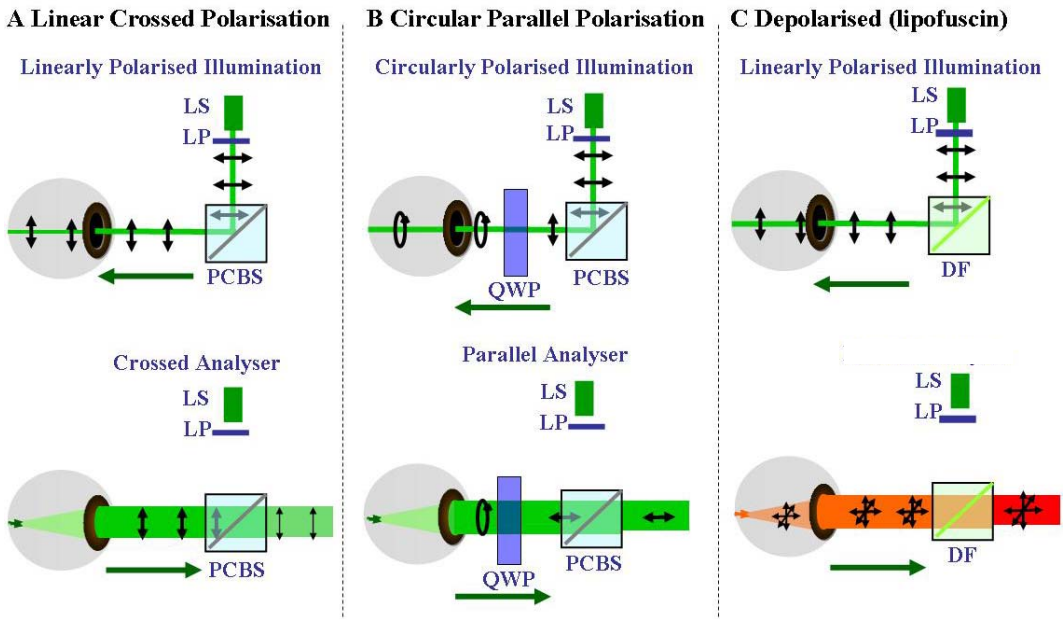

Figure 3.2. Configurations of the set-ups to obtain the different polarising conditions. (A) Linear crossed polarisation: linearly polarised light enters the eye, and light from the eye polarised in the perpendicular orientation is transmitted by the polarising beam splitter (PCBS) (crossed analyser), so that little light preserving the original polarisation orientation reaches the detector (see thinner arrows). (B) Circular parallel polarisation: light circularly polarised by a quarter wave plate (QWP) enters the eye, and light from the eye is linearly polarised in the orientation transmitted by PBS (parallel analyser). (C) Depolarised condition: partially polarised light enters the eye and stimulates lipofuscin molecules, which emit depolarised light that is transmitted by the dichroic filted (DF).

3.3.1.3.- Subjects

Twenty-eight subjects participated in the experiment. Ages ranged from 18 to 46 years and refractive errors ranged from –10.47 to 0.68 D. A total of 60 measurements (E#1-E#60). Both normal and atypically highly aberrated eyes were included, since the group under test includes 22 eyes after (at least one month) LASIK surgery, which typically increases the amount of higher order aberrations (Moreno-Barriuso et al., 2001b). Eleven eyes were tested both before and after LASIK, and were considered as independent measurements. The experimental protocol used was that described in section 2.4 of Chapter 2, for each polarisation condition.

3.3.2.- HARTMANN-SHACK

3.3.2.1.- Setup and procederes

The implementation of the HS wavefront sensor at Imperial College, London (Diaz-Santana and Dainty 1999, Diaz-Santana Haro, 2000), as well as the technique itself (Chapter 1, section 1.2.3) have been described in detail elsewhere. A schematic diagram of the HS sensor configuration used in this work is shown in Figure 3.3. The emerging beam was sampled by a rectangular lenslet array placed in a plane conjugate to the pupil. Each lenslet was 0.8 mm x 0.8 mm over the eye pupil and 35-mm focal length. The number of sampling lenslets (32 to 48 lenslets) was defined by the subject's pupil size (ranging from 5 mm to 6.5 mm). A CCD camera, placed on the focal plane of the lenslet array and conjugated with the retina recorded the HS spot pattern. Deviations from the ideal spot pattern are proportional to the local slopes of the wave aberration. The slopes were fitted to a 6^{th} order Zernike polynomial (27 terms) and the wave aberration was computed using a least-squares procedure. Same as for LRT, a LP and a PCBS were introduced in the setup, as well as a QWP or when required (see next section of this chapter), in order to induce the different polarisation conditions to study.

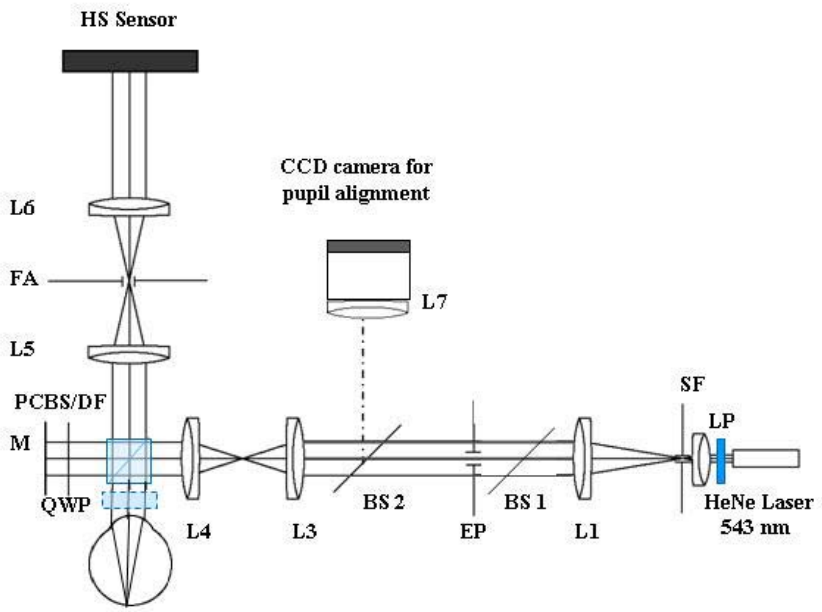

Figure 3.3. Schematic diagram showing the configuration of the HS sensor used in this study: LP is a linear polariser; SF is a spatial filter; L indicates lens; BS1 and BS2 are pellicle beam splitters; M is a mirror; EP is an entry pupil aperture (diameter=1.5 mm), and FA is a field aperture; PBS is a polarizing cube beam splitter, DF a dichroic filter, and QWP is a quarter wave plate which are combined in the setup to obtained the different polarising conditions.

3.3.2.2.- Experiments

The author did not participate in the experimental sessions, which took place at Imperial College (London), or in the data processing, but performed the analysis of the data from the different conditions. Three different experiments were performed, using different configurations for the state of polarisation in the illuminating channel, and state of polarisation of the light sampled in the imaging channel: 1) In the first experiment, the eye was illuminated with linearly polarised light (635 nm) and collected the light linearly polarised in the crossed direction. This was achieved by using a PCBS, which reflects linearly polarised light, and transmits linearly polarised light rotated 90^{o} (see Figure 3.2 A). 2) In the second experiment, the illumination channel was circularly polarised, and light with the same state of polarisation was maximally sampled in the imaging channel. This was achieved by placing a QWP between the PCBS and the eye (see Figure 3.2 B). 3) In the third experiment the eye was

illuminated using partially polarised light (from a He-Ne laser at 543nm), and completely depolarised light was sampled by the imaging channel. To achieve a depolarised state, a fluorescence technique was used (Delori et al., 1995, Diaz-Santana and Dainty 1999). Fluorescent light was collected by replacing the PCBS by a DF, reflecting the sampling light (543 nm) and transmitting wavelengths other than the excitation wavelength (see Figure 3.2 C). Fluorescence is known to originate in the lipofuscin molecules at the retinal pigment epithelium (see section 1.1.6 of Chapter 1). A fluorescent source is equivalent to a perfectly incoherent source. Light is completely unpolarised and speckle is not present. The peak of the fluorescent spectrum is close to 635 nm. All experiments were done foveally, and using the pupil centre as a reference. Subjects were stabilised with the help of a dental impression. Alignment was achieved by measuring the displacement required for the subject to stop seeing the beam coming into his/her eye on the left, right, top and bottom, and finally computing the pupillary centre. For each condition, at least ten measurements were obtained consecutively. The alignment procedure was repeated every ten measurements.

3.3.2.3.- Subjects

Eleven normal subjects participated in these experiments. Only left eyes were used (E#61-E#71). Ages ranged between 26 and 52 years. Spherical refractive errors ranged between -3.25 D and 2.25D. Seven subjects participated in comparative measurements of experiments 1 and 3; two subjects in comparative measurements of experiments 2 and 3; and two subjects in experiments 1 and 2. All eyes were dilated and cyclopleged with one drop of tropicamide 1% and one drop of phenylephrin 2.5% .

3.3.3.- COMPARISON OF HS AND LRT SET UPS

Previous studies have shown that measurements on the same normal subjects using HS and LRT techniques provide identical results, within the

accuracy of the methods (Moreno-Barriuso and Navarro, 2000, Moreno-Barriuso et al., 2001a). To test the equivalence of the two systems used in this study measurements were conducted on two control subjects who travelled between London and Madrid. These subjects did not participate in the full measurements reported in this study, and were tested with the standard conditions in each lab (543 nm illumination and linear polarisation with an arbitrary orientation for LRT, and 543 nm illumination and crossed polarisation for HS). Figure 3.4 shows wave aberration contour plots for the right eyes of both control subjects, for 3rd order and higher aberrations, for LRT (left panels) and HS (right panels). Pupil size was 6.5 mm in the LRT experiment and 6 mm in the HS experiment. Both systems captured similar wave aberration maps. The larger differences found for control eye #2 are likely due to slight differences in the alignment. RMS wavefront error for 3rd order aberrations and higher (computed for 6 mm pupils in both systems) was 0.46 μm and 0.43 μm for LRT and HS respectively, for control eye #1, and 0.48 μm and 0.57 μm, respectively for control eye #2. For both eyes, the SA 4^{th} order term was the major contributor to wavefront error: 0.30 μm and 0.33 μm for LRT and HS (control eye #1), and 0.28 μm and 0.35 μm for

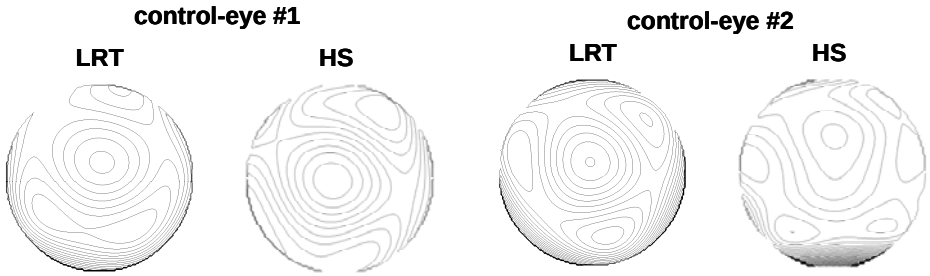

Figure 3.4. Wave aberration contour for control eyes measured in both the LRT setup in Madrid and the HS system in London. First- and second-order aberrations have been canceled. Pupil diameter was 6.5 mm for LRT and 6 mm for the HS. Contour spacing was 0.3 mm.

LRT and HS (control eye #2).

3.3.4.- STATISTICAL ANALYSIS

Despite discrete and limited sampling of the wave aberration (Wang and Silva, 1980), the Zernike polynomials can be considered practically orthogonal. A univariate statistical analysis (Student t-test) was therefore performed on each Zernike coefficient to assess possible differences across conditions, rather than performing a multivariate analysis (Hotelling t-squared test) on Zernike sets (Sokal and Rohlf, 1995). This allows us to assess whether some particular coefficients are more likely to show differences.

3.4.- **RESULTS**

3.4.1.- RAW DATA

LRT captures a set of retinal aerial images of a distant point source as a function of entry pupil position. An example of such a series of retinal images for a single run on Eye #23 for circularly parallel (A) and linearly crossed (B) polarisation conditions is shown in Figure 3.5 A and B, respectively. The images have been placed at their corresponding entry pupil position. The shape of aerial images (slightly defocused for this subject) remains approximately constant across the pupil for each condition. The relative intensity of the aerial images across the pupil is different in each condition: brighter in the centre in A, and brighter in the corners in B. Figure 3.5 C shows the corresponding retinal spot diagram of the sets of images in A (circles) and B (crosses), for this subject. Data across five consecutive runs have been averaged. The error bars indicate the standard deviation of the angular locations. For most positions, the difference between the two polarisation conditions is within the error. Figure 3.5 D and E shows HS images for circularly parallel (A) and

linearly crossed (B) polarisation conditions, for Eye #63. Figure 3.5 F shows the HS centroids corresponding to D (circles) and E (crosses). Despite the difference in brightness between both HS images, the centroid locations are very similar.

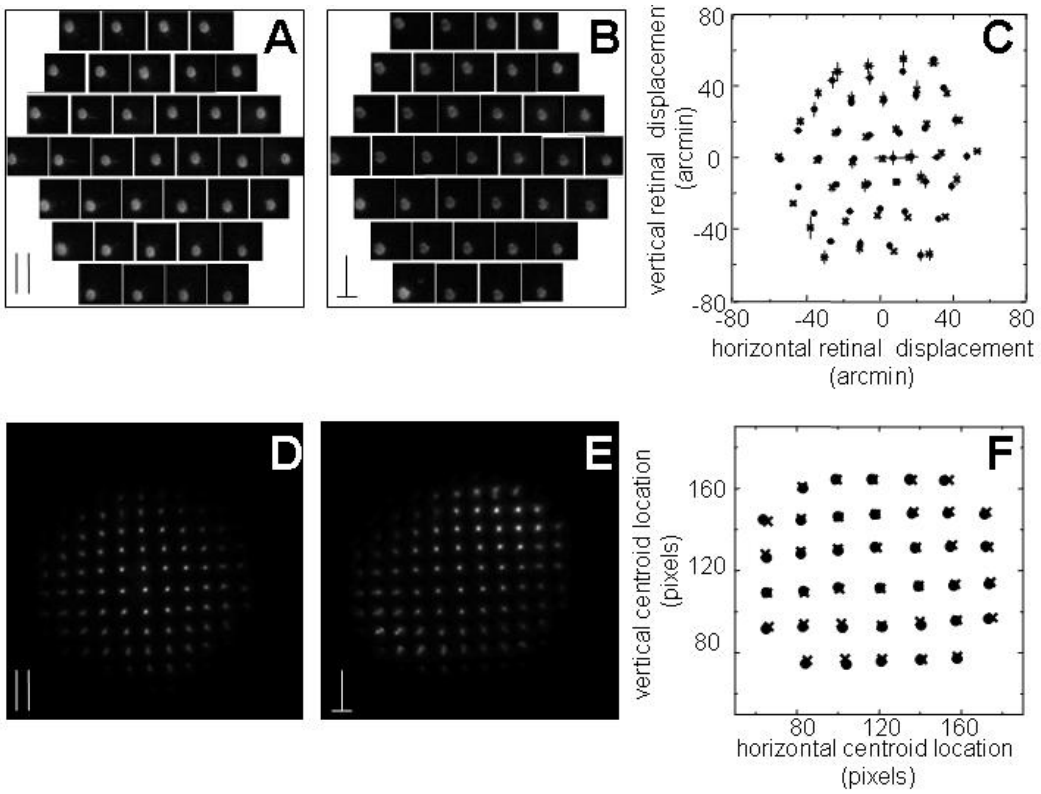

Figure 3.5. Raw data as captured by LRT (panels A–C) and HS (panels D-F) for different polarisation configurations. In LRT a series of retinal images is captured sequentially as a function of entry pupil position. Examples are shown for eye #23 for circular parallel polarization (A) and linear crossed polarization (B). Each image is placed at the corresponding entry location (as looking at the subject's pupil). Panel C shows the corresponding spot diagram of the images shown in A and B. Circles stand for circular parallel polarization and crosses for linear crossed polarization. Panels D and E show HS images for eye #63 for circular parallel polarization (D) and linear crossed polarization (E). Panel F plots the corresponding centroids of the HS images; symbol notation is the same as for the spot diagrams in C.

3.4.2.- INTENSITY PATTERNS

Figure 3.7 shows pupillary intensity patterns (intensity modulation of the raw images as a function of pupil position) corresponding to experiments 1 and 2 using a LRT, for 5 individual eyes (#24, #48, #23, #10). Each square represents the total intensity (average of 5 runs) of the aerial image of the corresponding pupil position. Pupil positions range from -3 to +3 mm both horizontally and vertically. Positive horizontal positions indicate nasal positions in right eyes and temporal positions in left eyes, and positive vertical positions indicate superior pupil. For each subject, data corresponding to the two polarisation combinations, crossed linearly polarised (experiment 1) and parallel circularly polarised (experiment 2), collected consecutively while keeping the rest of experimental conditions identical are shown. Each image is normalized to the maximum intensity value of the series. The intensity distribution changes completely depending on the polarisation combination. The parallel circularly polarised patterns (Figure 3.7, upper row) show a bright area in the central part of the pupil, with the location of the maximum depending on the subject, and the relative intensity decreasing towards the margins of the pupil. The crossed polarisation patterns (Figure 3.7, lower row) show a dark area in the central pupil, and bright areas at the corners of the pupil. It resembles the corneal cross, vignetted by the edges of the pupil, or the hyperbolic shape associated with corneal birrefringence, and observed when the cornea is imaged through two crossed polarisers (Van Blokland and Verhelst, 1987, Stanworth and Naylor, 1950, Cope et al., 1978) (Figure 1.12 B in Chapter 1). As found in previous studies (Van Blokland and Verhelst, 1987) these intensity patterns show bilateral mirror symmetry (Figure 3.6, for right and left eye of the same subject).

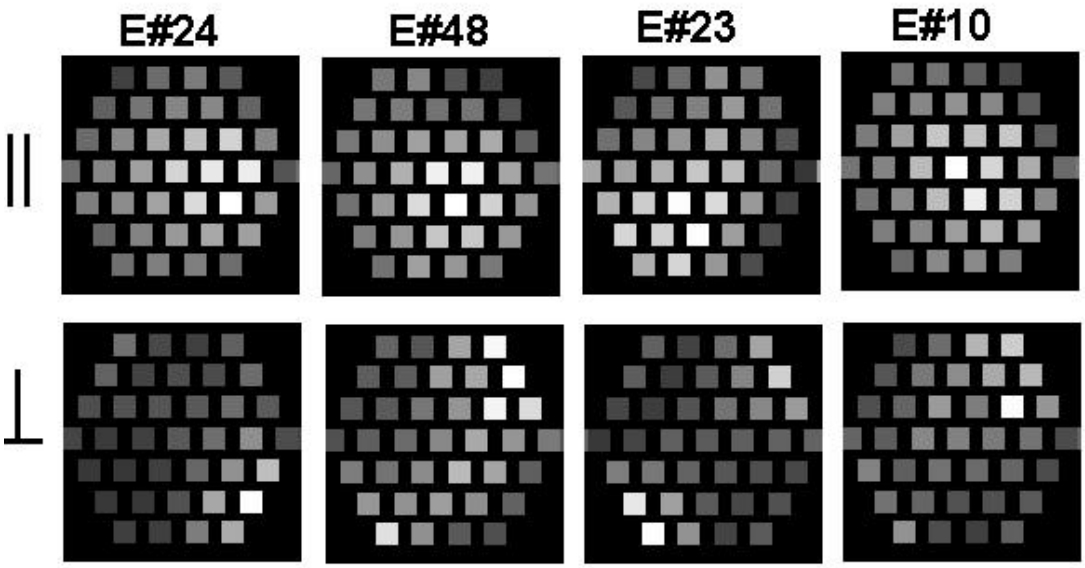

Figure 3.7. Pupillary intensity maps computed from the intensity of the LRT aerial images for eyes #24 (OS); #48 (OD); #23 (OS) and #10 (OD). Each square represents the total intensity (average of five runs) of the aerial image of the corresponding pupil position. Upper row, circular polarization in the illumination channel, analyzer in the same orientation. Lower row, linear polarization in the illumination channel, analyzer in the crossed orientation. Pupil positions range from 23 to 13 mm. Right horizontal positions indicate nasal positions in right eyes and temporal positions in left eyes, and superior vertical positions indicate superior pupil.

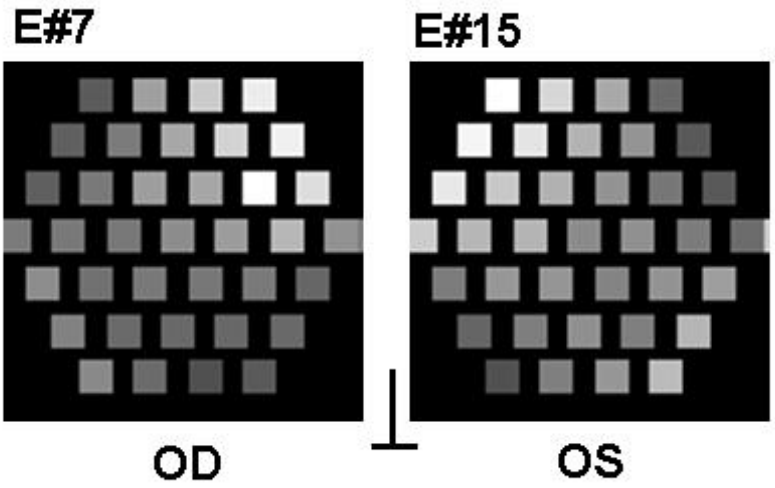

Figure 3.6. Pupillary intensity maps (computed from LRT aerial images, as in Figure 3.5) for right (E#7) and left (E#15) eyes of the same subject, using linear crossedpolarisation. The maps show a dark central area and bright nasal-superior corners, and they are bilaterally symmetric.

Figure 3.8 shows the HS spot patterns, for 3 different eyes (all left eyes). Upper and lower rows represent data corresponding to different conditions of state of polarisation. Left panels show cross-polarised (top) and autofluorescence (bottom) patterns for eye #67; middle panels show parallel circular polarisation (top) and autofluorescence (bottom) for eye #71; and right panels show parallel circular (top) and crossed (bottom) polarisations for eye #63. Intensity patterns in the crossed polarised and parallel circular contributions are similar to those described for Figure 3.7. The autofluorescence spot patterns show the most homogenous intensity distribution.

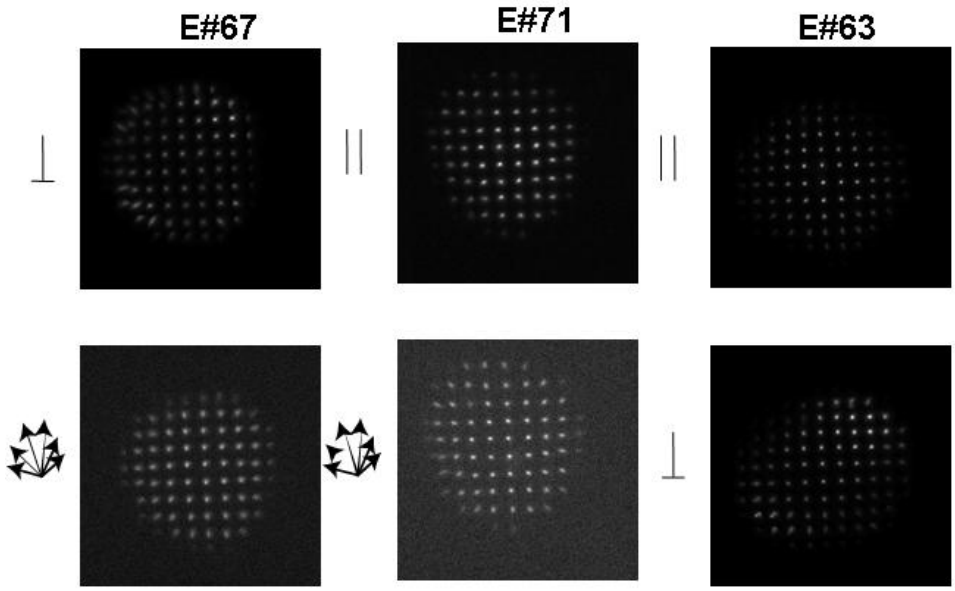

Figure 3.8. Hartmann-Shack spot image for eyes #67 (OS), #71 (OS), #63 (OS).

The left panels compare linear polarization in the illumination channel and analyzer in the crossed orientation (top) with autofluorescence (totally depolarized) sampled light (bottom). The middle panels compare circular polarization in the illumination channel and analyzer in the parallel orientation (top) with autofluorescence (bottom). The right panels compare circular parallel (top) with linear crossed polarizations (bottom). Right horizontal positions indicate temporal pupil positions, and superior vertical positions indicate superior pupil. See (Marcos et al., 2002)

3.4.3.- WAVE ABERRATION PATTERNS

Figure 3.9 A shows contour plots of the wave aberration corresponding to the four typical eyes and the two experimental conditions shown in Figure 3.5, measured using LRT. Each map is the

average of at least three experimental runs. Tilt and defocus were set to zero. Eyes #24 (OS) and #48 (OD) are eyes following LASIK refractive surgery; Eyes #23 (OS) and #10 (OD) are normal eyes. Figure 3.9 B shows contour plots of the wavefront aberration corresponding to 3 eyes measured with HS (#67, #71 and #70) and combinations of experimental conditions shown in Figure 3.8. Wave aberration patterns of the same eyes are quite similar for the different conditions.

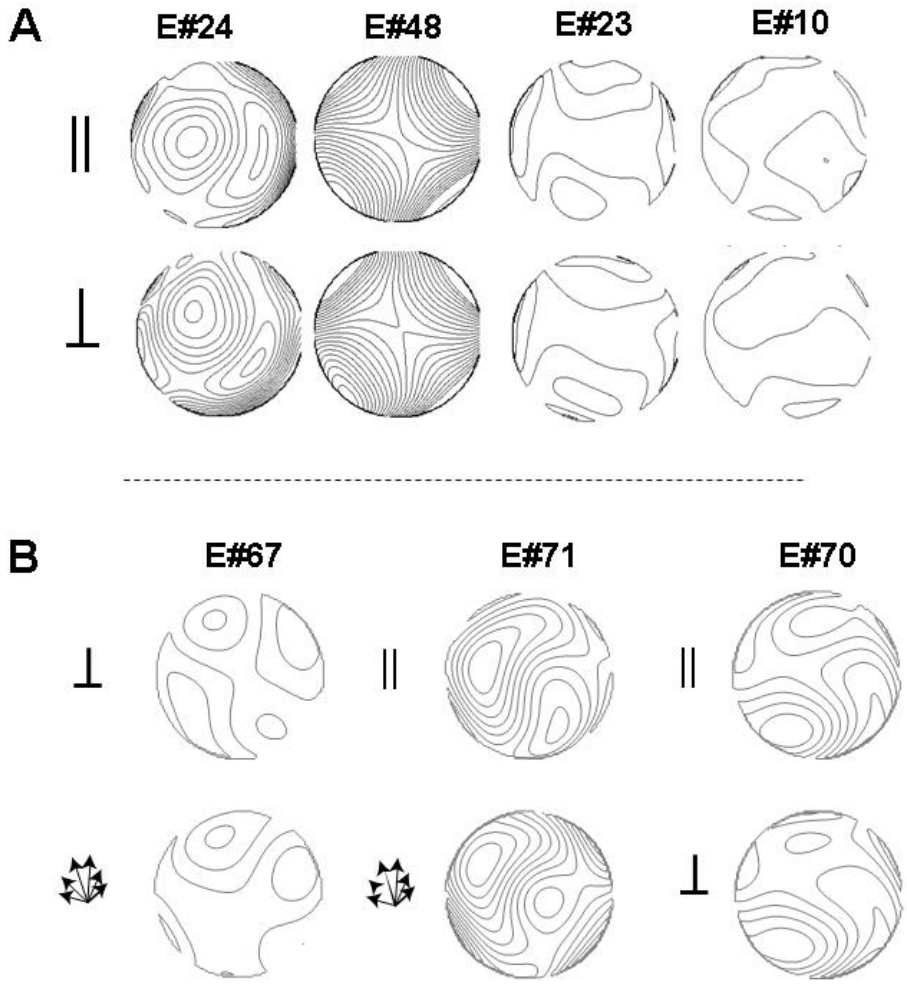

Figure 3.9. Wave aberration contour maps for some of the eyes measured with LRT (A) and HS (B).

(A) For eyes #24, #48, #23, and #10, measured with LRT, lines are plotted every 1 μm. Upper and lower panels as in Figure 3.7. Defocus has been removed. Pupil diameter was 6.5 mm for all eyes. (B) For eyes #67, #71, and #70, measured with the HS lines are plotted every 0.2 μm. Polarization combinations as explained in Figure 3.8. Tilt and defocus have been removed. Pupil diameter was 6.5 mm for #67 and #71 and 6 mm for #70.

3.4.4.- ZERNIKE COEFFICIENTS

Figure 3.10 shows examples of comparisons of Zernike coefficients measured with different pairs of polarisation states, for one of the eyes shown in Figure 3.9 A and the three eyes of Figure 3.9 B: (A) E#23, OD, measured with linear crossed polarisation (crosses) and circular parallel polarisation (circles), using LRT; (B) E#71, OS, measured with circular polarisation (circles) and fluorescence mode (triangles), using HS; (C) E#67, OS, measured with crossed linear polarisation (crosses) and fluorescence mode (triangles), using HS; and (D) E#70, OS, measured with crossed linear polarisation (crosses) and circular polarisation (circles), using HS. Error bars indicate the mean standard deviation. The Zernike coefficient patterns vary substantially across individuals, but measurements on the same subject differing only by the polarisation states are very similar. The discrepancy in defocus term at Figure 3.10B is due to autofluorescence light coming from a deeper retinal layer.

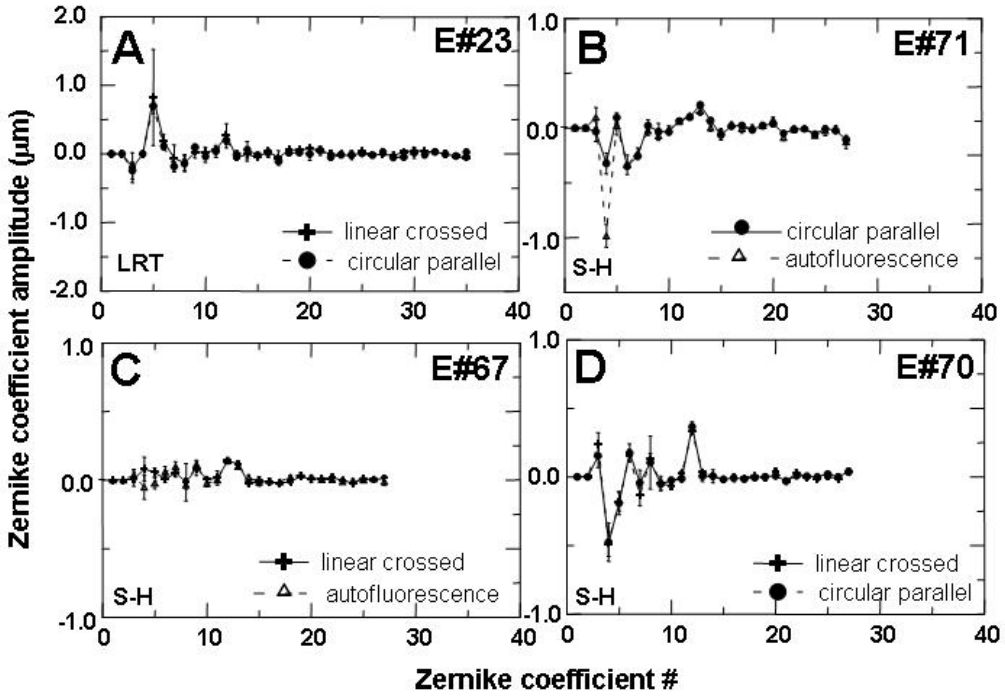

Figure 3.10. Zernike coefficients for eye #23 from Figure 3.9 A (A) and the three eyes (#71, #67, #70) from Figure 3.9 B (B)– (D), comparing different combinations of polarization conditions. Each symbol is the average of several measurements in the same conditions. Error bars stand for the mean std.

Figure 3.11 shows examples of individual coefficients Z_2^0 (A), Z_2^{-2} (B), Z_3^1 (C), and Z_4^0 (D), for the 60 eyes and the two experimental conditions of the LRT measurements (left panels) and the 11 eyes and three experimental conditions of the HS measurements (right panels). Eyes are ranked by decreasing defocus coefficient (from higher to lower myopes).

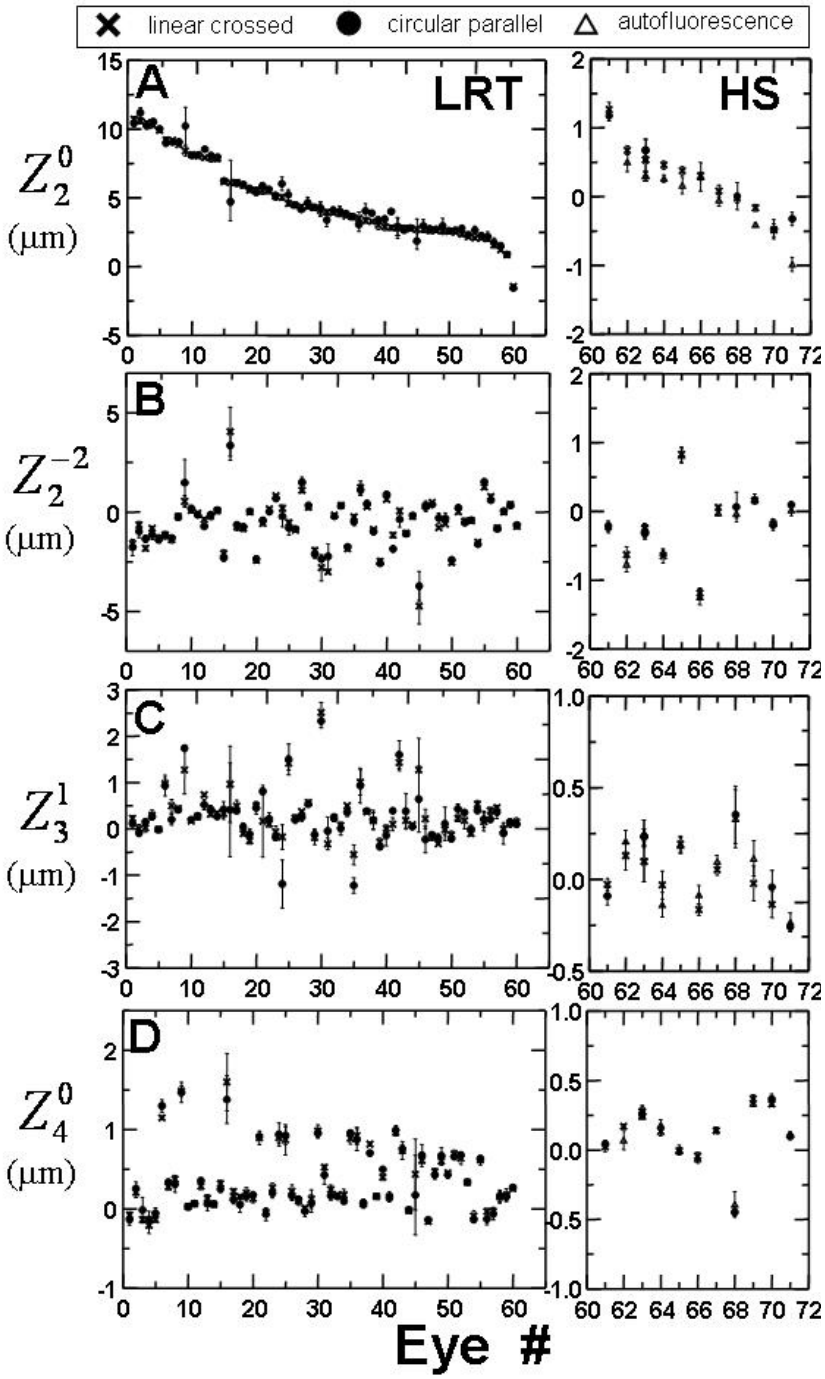

Figure 3.11. Zernike coefficients Z_2^0 (A), Z_2^{-2} (B), Z_3^1 (C), and Z_4^0 (D), for all eyes of this study (E#1–60 measured with LRT and E#61–71 with the HS), comparing at least two different polarization states (represented by different symbols). Error bars stand for the mean std.

For the 60 eyes measured with the LRT, only 44 coefficients out of 1980 (60 x 33 terms), i.e. 2.2%, showed statistically significant differences (t-test $p<0.001$) between the linear crossed and circular parallel polarisation. The defocus term (Z_2^0) was significantly different in 7 eyes. This term along with Z_3^{-3} was the one showing differences in more eyes (8.5%). A least square difference multiple comparison test showed only significant differences ($p=0.0002$) on the defocus term. The mean standard deviation of the Zernike coefficients (averaged across subjects and Zernike terms) was 0.065 μm, averaging the standard deviations obtained for each polarisation state. When pooling together data from all polarisation states, the mean standard deviation of the Zernike coefficients was 0.077 μm, only slightly higher than within the same polarisation state. For the 11 eyes measured with HS, 37% of the coefficients showed statistically significant differences (t-test, $p<0.001$) between linear crossed and autofluorescence, 37% between circular parallel and linear crossed polarisation and 46% between circular parallel and autofluorescence. Comparing sets of measurements under similar polarisation conditions, but repositioning the subject between sets of 10 consecutive runs provided similar percentages of significantly different (t-test, $p<0.001$) coefficients: 40% comparing linear crossed polarisation sets of measurements, 52% for circular parallel, and 60% for autofluorescence. The mean std of the Zernike coefficients (across all polarisation conditions) was 0.126 μm, within a single polarisation state was 0.102 μm on average, and across identical consecutive runs was 0.039 μm.

3.5.- **DISCUSSION**

It has been shown that when using different states of polarisation in the illumination and detection channels, the intensity of the retinal images captured by imaging aberrometers depended on the position over the pupil of the entry (or exit) ray. This modulation depended on both the

pupil relative luminous efficiency, in case of light interacting with cone photoreceptors (Burns et al., 1995) and the interaction of the state of polarisation with birefringence properties, particularly those of the cornea (Van Blokland and Verhelst, 1987, Stanworth and Naylor, 1950, Cope et al., 1978). Retinal polarisation effects were probably irrelevant, since the foveal area sampled (a few minutes of arc) was much smaller than the retina brushlike patterns (4-5^{o}) observed in retinal photographs between polarisers, which are attributed mainly to the retinal fibre layer. In addition, retardation by photoreceptors as suggested by Hocheimer & Kues (Hocheimer and Kues, 1982) has been proved small (Van Blokland, 1986). Whereas the crossed polarisation patterns (polarisation cross) seems related to corneal birefringence, the Gaussian distribution observed in parallel circularly polarised patterns is very likely associated with directionality properties of the cone photoreceptors (Burns et al., 1995, Marcos and Burns, 1999, Marcos et al., 2000).The autofluorescence spot patterns show the most homogenous intensity distribution, consistent with the fact that cones do not recapture light scattered by lipofuscin (Burns et al., 1997).

However, in spite of the effect of polarisation on the intensity distribution of the images, this had little effect on the aberrations measured, within the accuracy and sampling density of the technology used. The larger statistical differences found across Zernike coefficients obtained with different polarisation states for HS measurements are very likely due to differences in alignment between measurements, and not differences intrinsic to the polarisation state. The larger variability of the autofluorescence data is likely due to the lower signal to noise associated to this type of measurements (Diaz-Santana and Dainty 1999).

The fact that ocular aberrations measured using imaging methods, such as the LRT or HS, are insensitive to polarisation has important practical implications. For example, when building such an instrument,

one can choose the polarisation states for illumination and detection that result in the best light efficient configuration, or that which avoids reflections or artefacts. This differs from conventional double-pass measurements, where differences in polarisation produced variations in the PSF and MTF (Bueno and Artal, 1999, Gorrand et al., 1984, Gorrand, 1979).

Published data obtained using the SRR also show that ocular aberrations do not depend on the state of polarisation (Prieto et al., 2001). This is a psychophysical technique, and the subjects did not perceive differences as a linear polariser in the test channel was moved, for any of the pupil locations under test. These results, along with those shown in the present study, suggest that the differences in retardation across the pupil imposed by corneal birefringence, produce non-significant phase delays compared to those produced by aberrations, at least within the accuracy of the measurements. Interestingly, these results also hold for patients following LASIK surgery. Along with a change in corneal shape, producing a significant increase of aberrations (see Chapter 7), these patients may have suffered a change in corneal birrefringence due to re-organization of stromal collagen fibrils induced by surgery (Farrell et al., 1999, Meek and Newton, 1999, Brinkmann et al., 2000). Even if only a fraction of stromal fibres undergo reorganization, the stromal bed is substantially reduced in the higher myopic patients. However, the intensity distribution patterns obtained by LRT did not change with surgery (neither for crossed linear or parallel circular polarisations). This is in agreement with Bueno et al. (2006), who measured four normal and four post-LASIK young eyes using an aberropolariscope. However, although they found no differences in aberration measurements for different polarisation states in both groups, they did find changes in the polarisation characteristics. Post-LASIK eyes showed larger levels of depolarisation and more irregular patterns of retardation and corneal slow axis.